

Energy Cost for Flocking of Active Spins: The Cusped Dissipation Maximum at the Flocking Transition

Qiwei Yu^{1,2} and Yuhai Tu¹

¹*IBM T. J. Watson Research Center, Yorktown Heights, New York 10598, USA*

²*Lewis-Sigler Institute for Integrative Genomics, Princeton University, Princeton, New Jersey 08544, USA*

 (Received 25 May 2022; revised 23 August 2022; accepted 28 November 2022; published 28 December 2022)

We study the energy cost of flocking in the active Ising model (AIM) and show that, besides the energy cost for self-propelled motion, an additional energy dissipation is required to power the alignment of spins. We find that this additional alignment dissipation reaches its maximum at the flocking transition point in the form of a cusp with a discontinuous first derivative with respect to the control parameter. To understand this singular behavior, we analytically solve the two- and three-site AIM models and obtain the exact dependence of the alignment dissipation on the flocking order parameter and control parameter, which explains the cusped dissipation maximum at the flocking transition. Our results reveal a trade-off between the energy cost of the system and its performance measured by the flocking speed and sensitivity to external perturbations. This trade-off relationship provides a new perspective for understanding the dynamics of natural flocks and designing optimal artificial flocking systems.

DOI: [10.1103/PhysRevLett.129.278001](https://doi.org/10.1103/PhysRevLett.129.278001)

Understanding how collective coherent motion (“flocking”) emerges from a system of self-propelled, interacting individuals has been a central question in nonequilibrium statistical physics and biophysics [1–3]. Familiar examples include birds, fish, bacteria [3,4], and synthetic systems such as active colloids [5]. Theoretical studies have involved models of self-propelled, aligning particles with continuous [6–10] or discrete [11,12] symmetry. Despite their diversity, these systems are all far from thermodynamic equilibrium [13] and thus a continuous dissipation of free energy is required to create and maintain the long-range flocking order. Indeed, energy dissipation plays a crucial role in driving living systems out of equilibrium to achieve important biological functions, such as adaptation [14], error correction [15–20], spatial patterns [21], and temporal oscillation [22]. Here, we study nonequilibrium thermodynamics of dry aligning active matter [23], aiming to elucidate the relationship between the energetic cost of flocking and its performance measured by the flocking speed and sensitivity.

The dynamics and energy dissipation (entropy production) of flocking can be studied at the microscopic level by prescribing the single-particle dynamics [6] or at the coarse-grained level with hydrodynamic field theories [7,8]. In the latter case, the entropy production rate (EPR) calculated from the standard procedure gives a measure of irreversibility but usually has no thermodynamic interpretation (unless under special conditions such as linear irreversible thermodynamics [24]). Namely, it does not give the (physical) heat dissipation rate, and an alternative term “information EPR” has been proposed to differentiate it from the microscopic EPR, which has

unambiguous thermodynamic interpretation [25–27]. The reason behind this discrepancy is that coarse graining drastically decreases the dissipation rate [28–30], which means that macroscopic theories tend to dramatically underestimate the energy dissipation. Therefore, it is fundamentally important to elucidate the energy cost of flocking using a microscopic model, which gives the “true” heat dissipation, despite existing work using hydrodynamic approaches [31,32].

Here, we investigate the energy dissipation of the active Ising model (AIM) [11,12], which describes a lattice gas of Ising spins with ferromagnetic alignment and biased diffusion. Our main finding is a cusped energy dissipation maximum at the flocking transition point, which is supported by numerical simulations and confirmed by the analytical solution of reduced AIMs with two or three sites. These findings uncover a new perspective on the energy-speed-sensitivity trade-off in flocking.

Dissipation in the active Ising model.—The 2D AIM describes N particles on an $L_x \times L_y$ lattice with periodic boundary conditions. Each particle carries an Ising spin $s = \pm 1$, and the number of \pm spins on site (i, j) is denoted by $n_{i,j}^{\pm}$ (no volume exclusion). The system follows continuous-time Markovian dynamics including flipping (local alignment) and hopping (self-propulsion). Each particle can flip its spin from s to $(-s)$ at rate $\omega e^{-\beta E_0 s m_{i,j} / \rho_{i,j}}$, where $m_{i,j} = n_{i,j}^+ - n_{i,j}^-$ and $\rho_{i,j} = n_{i,j}^+ + n_{i,j}^-$ are the local magnetization and density, respectively. ω^{-1} sets the flipping timescale. E_0 measures the strength of the spin-spin alignment interaction, and β is the inverse temperature which is set to 1. Each spin can also hop to one of the four

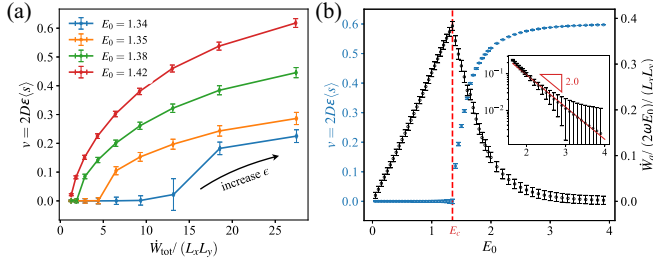


FIG. 1. (a) The average flocking speed v versus the total dissipation \dot{W}_{tot} for fixed values of E_0 and increasing ϵ . (b) The average flocking speed (blue) and alignment dissipation (black) for $\epsilon = 0.3$. The red dashed line is the transition point E_c above which $v > 0$. The inset shows the exponential decay of dissipation at large E_0 . $L_x = 300$, $L_y = 100$, $\bar{\rho} = N/(L_x L_y) = 5$, $D = 1$, and $\omega = 1$. See Sec. I A in the Supplemental Material for details [33].

neighboring sites, at rate $D(1 + \epsilon)$ to the right, $D(1 - \epsilon)$ to the left, and D to up and down. The flipping dynamics obeys detailed balance according to the Hamiltonian of a fully connected (mean-field) Ising model, but the hopping dynamics breaks detailed balance and drives the system out of equilibrium. Flocking is defined as the emergence of long-range order (LRO) among spins characterized by a finite $\langle s \rangle$ with the mean flocking speed given by $v = 2D\epsilon\langle s \rangle$ in the x direction. Note that, in the special case of unbiased diffusion $\epsilon = 0$, LRO can still emerge albeit with zero flocking speed (see Fig. S3 in the Supplemental Material for details [33]).

Two equivalent approaches are employed to calculate the steady-state entropy production (energy dissipation) rate. The first method calculates the average dissipation rate from the ratio of forward and backward realizations of a sufficiently long trajectory (assuming ergodicity) obtained by simulating the AIM dynamics [34]. The second approach considers the different spin configurations ($\{n_{i,j}^\pm\}$) as states of a reaction network with flipping and hopping as the two types of transitions between different states. Once the AIM reaction network reaches its nonequilibrium steady state, the dissipation rate can be determined by following the standard procedure for computing entropy production rate of reaction networks [35,36]. These two approaches are equivalent. The former is suited for the numerical simulation of the full AIM, and the latter offers analytical tractability in the two-site (and three-site) AIM.

A finite amount of energy dissipation is needed to drive the system sufficiently away from equilibrium to generate flocking behavior. As shown in Fig. 1(a), a nonzero flocking speed v can be achieved by increasing ϵ at fixed E_0 , which also increases the total dissipation rate \dot{W}_{tot} . The flocking motion does not emerge until \dot{W}_{tot} is above a certain (nonzero) threshold.

The total dissipation rate can be decomposed into contributions from the two types of transitions:

$\dot{W}_{\text{tot}} = \dot{W}_m + \dot{W}_a$, where \dot{W}_m and \dot{W}_a correspond to the dissipation rates due to motion (hopping) and alignment (flipping) of the particles, respectively. Since each particle moves at an average speed $v_0 = 2D\epsilon$ and each step along the bias direction costs energy $\ln[(1 + \epsilon)/(1 - \epsilon)]$, the resulting dissipation rate for motion is simply $\dot{W}_m = Nv_0 \ln[(1 + \epsilon)/(1 - \epsilon)]$ (see Appendix A for details). The alignment dissipation \dot{W}_a can be calculated by summing up the cost of all flipping events during a sufficiently long time interval τ ,

$$\dot{W}_a = \lim_{\tau \rightarrow \infty} \frac{1}{\tau} \sum_{0 < t < \tau} 2E_0 \frac{1 - m_{i,j} s}{\rho_{i,j}}. \quad (1)$$

Each event flips a spin s to $(-s)$ on site (i, j) , which has local magnetization $m_{i,j}$ and local density $\rho_{i,j}$ (see Appendix A). It will be convenient to henceforth refer to the nondimensionalized alignment dissipation rate $\dot{w}_a = \dot{W}_a/(2\omega E_0)$ as the alignment dissipation.

The motion dissipation rate \dot{W}_m is responsible for driving the self-propulsion of the particles, which is independent of the alignment dynamics. As expected, \dot{W}_m increases monotonically with ϵ , vanishing in the unbiased limit ($\epsilon = 0$) and diverging in the irreversible limit ($\epsilon \rightarrow 1$). The origin of the alignment dissipation \dot{W}_a is more subtle. Although the local spin flipping dynamics obeys detailed balance, the local spin system at a given site is driven out of equilibrium by the continuous exchange of spins between neighboring sites due to the transport process. A continuous dissipation rate \dot{W}_a is needed to drive the spin alignment to maintain the flocking order. As a result, \dot{W}_a depends on both the alignment strength (E_0) and the particle's key transport properties, in particular, the motion bias ϵ and the relative timescale D/ω . Next, we investigate how the flocking behavior and dissipation rates depend on these key control parameters of the system ($E_0, \epsilon, D/\omega$).

A cusped dissipation maximum at the flocking transition.—For a fixed bias ϵ , the system remains disordered ($v = 0$) until E_0 is increased above a certain threshold E_c [Fig. 1(b)]. The alignment dissipation \dot{w}_a increases linearly in the disordered phase and decreases monotonically in the flocking phase (exponentially at large E_0 as shown by the inset). Remarkably, it reaches maximum exactly at the transition point E_c in the form of a cusp. The value of \dot{w}_a is continuous across the transition, but its derivative ($d\dot{w}_a/dE_0$) changes abruptly from positive to negative across E_c , forming a cusp at its maximum. Since \dot{W}_m stays constant, the same cusped maximum behavior also exists for \dot{W}_{tot} . Extensive numerical simulations find this behavior to be general, regardless of the bias ϵ or the relative timescale set by D/ω (see Appendix A). The critical E_c decreases with ϵ and increases with ω , but it always coincides with the maximum of \dot{w}_a . The alignment

dissipation can be decomposed into the product of the frequency of flipping events \dot{n}_f and the mean energy cost per flip $\dot{w}_f = \dot{w}_a / \dot{n}_f$. At the transition point, they both have continuous values but discontinuous first derivatives, which results in the cusp of \dot{w}_a (see the Supplemental Material [33]).

As discussed previously, the key to understanding the alignment dissipation is how the transport of spins between neighboring sites drives the local spin system out of equilibrium. However, it is difficult to understand the full AIM with a large system size due to the numerous degrees of freedom. Next, we investigate the alignment dissipation in a reduced AIM with the minimal number of sites that allows transport of active spins.

The two-site (and three-site) AIM shows the cusped maximum of flocking dissipation.—We consider a special case of the AIM with only two sites ($L_x = 2$ and $L_y = 1$), which is the minimum system size needed to drive the AIM out of equilibrium to produce flocking behavior. The flipping and hopping dynamics are the same as the full AIM. Importantly, hopping left- and rightward are considered to be two different processes, even though they reach the same site due to the periodic boundary condition. In the flocking phase, the left-right symmetry is spontaneously broken and hopping in one direction dominates. Conceptually, the two-site AIM can be considered as a coarse-grained version of the full AIM. It retains much of the physics of the full AIM, including the flocking transition and the associated dissipation maximum.

The model is fully characterized by the total number of spins N and three state variables (a_0, a_1, b_1) , where a_0 is the total number of + spins; a_1 and b_1 correspond to the number of + and - spins on site 1, respectively. The dynamics of the probability distribution $P(a_0, a_1, b_1)$ is governed by the master equation,

$$\frac{dP(a_0, a_1, b_1)}{dt} = \mathcal{L}P(a_0, a_1, b_1), \quad (2)$$

where \mathcal{L} is a linear operator (matrix) capturing the transitions. (The full equation and its solution are covered in the Supplemental Material, Sec. II [33].) The steady-state distribution $P^s(a_0, a_1, b_1)$ can be found by solving $\mathcal{L}P^s(a_0, a_1, b_1) = 0$ subject to normalization $\sum_{a_0, a_1, b_1} P^s(a_0, a_1, b_1) = 1$ and can be used to compute all statistical properties of the system, e.g., the average total magnetization $\langle m \rangle = \sum_{a_0, a_1, b_1} (2a_0 - N) P^s(a_0, a_1, b_1)$.

At finite N , the phase transition point E_c can be determined by computing the effective free energy landscape $F(m) = -\ln P(m)$, where $P(m) = \sum_{a_0, a_1, b_1} \delta(2a_0 - N - m) P^s(a_0, a_1, b_1)$ is the steady-state distribution of the total magnetization m . As shown in Fig. 2(a), as E_0 increases, the disordered state $m = 0$ goes from stable [$F''(0) > 0$] to unstable [$F''(0) < 0$], indicating the emergence of flocking. The transition point E_c [determined by

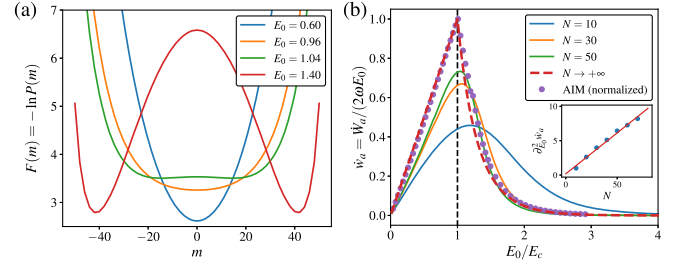


FIG. 2. (a) The effective free energy landscape demonstrates the existence of a nonequilibrium phase transition in the two-site AIM. $N = 50$, $D = \omega = 1$. (b) The alignment dissipation of the two-site AIM with different finite N (solid lines) and infinite N (red dashed line) and the full AIM (purple dots, normalized according to the text). Inset: the curvature at the dissipation maximum in the two-site AIM.

$F''(0) = 0$] and the position of the alignment dissipation maximum ($E_m = \text{argmax}_{E_0} \dot{w}_a$) are extrapolated to converge at infinite N (see the Supplemental Material, Fig. S3 [33]). Moreover, the curvature at the peak $\partial_{E_0}^2 \dot{w}_a|_{E_0=E_m}$ increases with N [Fig. 2(b) inset] and it is projected to diverge at infinite N . These results indicate a cusped dissipation maximum at flocking transition of the two-site AIM, consistent with observation in the full AIM.

In the infinite N limit, the steady-state probability P^s can be obtained analytically by assuming $D \gg \omega$. However, this assumption is not essential to the results. Perturbation theory shows that higher-order corrections of the order $\mathcal{O}(\omega/D)$ do not affect the cusped maximum behavior in \dot{w}_a (see Appendix B). The effective free energy in the limit $\omega/D \rightarrow 0$ is

$$\frac{F(m)}{N} = z \ln z + (1 - z) \ln(1 - z) + 2E_0 z(1 - z) + \mathcal{O}(N^{-1}), \quad (3)$$

where $z = a_0/N = (N + m)/(2N)$ is the fraction of spin-up. The flocking transition takes place at $E_c = 1$, where the most probable state (saddle point) goes from the disordered state ($z = \frac{1}{2}$) to the flocking state with $z = z^* (\neq \frac{1}{2})$, where z^* is determined by

$$\frac{1}{2(1 - 2z^*)} \ln \frac{1 - z^*}{z^*} = E_0, \quad (E_0 > 1), \quad (4)$$

which has two solutions z^* and $(1 - z^*)$ corresponding to flocking left- and rightward, respectively. Although the free energy is equivalent to that of the mean-field Ising model, the system continuously dissipates energy due to non-vanishing state-space fluxes. The fluxes associated with flipping give the alignment dissipation,

$$\dot{w}_a = \frac{1}{2\omega E_0} \sum_{\text{flip}} (J_+ - J_-) \ln \frac{k_+}{k_-} = \sum \sigma P^s \equiv \langle \sigma \rangle, \quad (5)$$

where σ is the local alignment dissipation rate whose average over P^s gives the steady-state alignment dissipation \dot{w}_a . The averaging is computed using the saddle point method, which expands σ around the most probable state. Importantly, direct evaluation of σ at the

saddle point vanishes, and the leading-order contribution comes from expansion to the second order in (a_1, b_1) . This indicates that particle number fluctuations are the essential source of alignment dissipation, which can be expressed as

$$\dot{w}_a = \frac{1}{2} \left[\frac{\partial^2 \sigma}{\partial a_1^2} \langle (a_1 - a_1^*)^2 \rangle + \frac{\partial^2 \sigma}{\partial b_1^2} \langle (b_1 - b_1^*)^2 \rangle \right] = \begin{cases} E_0 + \mathcal{O}(\frac{\omega}{D}), & 0 < E_0 < E_c (= 1) \\ 8E_0 [z^* (1 - z^*)]^{3/2} + \mathcal{O}(\frac{\omega}{D}), & E_0 \geq E_c \end{cases}, \quad (6)$$

where the derivatives are evaluated at the saddle point $(a_0^*, a_1^*, b_1^*) = (z^*N, z^*N/2, (1 - z^*)N/2)$. The explicit expressions for the $\mathcal{O}(\omega/D)$ terms can be found in Appendix B and the Supplemental Material [33].

It is clear from Eq. (6) that $\partial_{E_0} \dot{w}_a$ is discontinuous at the critical point ($E_0 = E_c$) because $\partial_{E_0} z^*$ is discontinuous there. Quantitatively, we have $\partial_{E_0} \dot{w}_a|_{E_0=1^-} = 1$ and $\partial_{E_0} \dot{w}_a|_{E_0=1^+} = -3.5$, which shows that \dot{w}_a [red dashed line in Fig. 2(b)] exhibits a cusped maximum exactly at $E_c = 1$. Equation (6) explicitly connects the dissipation \dot{w}_a to number fluctuations [$\langle (a_1 - a_1^*)^2 \rangle$ and $\langle (b_1 - b_1^*)^2 \rangle$].

To make a direct comparison between the two-site AIM and the full AIM, we rescale E_0 by E_c , normalize the dissipation by its maximum, and plot them against each other in Fig. 2(b). The two models agree exactly in the disordered phase where dissipation grows linearly with E_0 , as well as deep in the flocking phase where dissipation decays exponentially to zero. The cusped maximum at transition is also in good agreement, evident from the discontinuity of the slope. There is a small quantitative difference in dissipation at E_0 slightly above E_c because the two-site model cannot capture the flocking band structure in the mixed phase [37].

Although the two-site AIM captures the flocking transition and the cusped dissipation maximum of the full AIM, \dot{w}_a does not depend on the bias ϵ [Eq. (6)] since hopping to the left and to the right end up at the same site. To make sure this special property of the two-site model does not affect the general results, we extend the analytical solution to the three-site AIM. Aside from being more tedious, the three-site AIM can be solved in a similar fashion as the two-site AIM (see Appendix B and the Supplemental Material for details [33]), which not only confirms the existence of the cusped dissipation maximum at the flocking transition, but also captures the dependence of \dot{w}_a on ϵ explicitly.

The energy-speed-sensitivity trade-off.—The flocking of interacting particles is conceptually analogous to the synchronization of coupled oscillators [38,39], which can be understood as flocking (collective dynamics) of the phases of individual clocks. In both cases, an extra energy dissipation is needed to maintain coherence among individual subsystems (spins or oscillators) that are already out of equilibrium. However, the dissipation of these two

systems exhibits different behaviors. For coupled oscillators, the dissipation increases with the order parameter, meaning that it is very costly to maintain a system of highly coupled (and therefore synchronized) oscillators [39]. In the AIM, however, dissipation peaks exactly at the transition and decreases with interaction (E_0) in the flocking phase. At large E_0 , the highly ordered flock requires a smaller energy to maintain. The difference between the two behaviors stems from the alignment mechanisms. The active spins align locally, which effectively synchronizes their velocities. The coupled oscillators are synchronized by exchanging phases, whose analogy in the AIM would be simultaneous displacement of pairs of particles. This non-local interaction couples the alignment cost to the cost of motion (i.e., advancing the individual clocks), leading to a higher dissipation in the ordered phase. These analyses suggest that, compared to exchanging position, local alignment of velocity is an energetically more favorable way of maintaining the order in a system of active particles.

Another key property of flocks is its sensitivity to external perturbations, which we characterize by the magnetic susceptibility χ of the AIM. In AIM, there are many choices of parameters (ϵ, E_0) to achieve any given flocking speed v as shown in Fig. 3(a). For a given v , the total dissipation achieves its minimum in the limit of $E_0 \rightarrow \infty$ and $\epsilon \rightarrow v/(2D)$, which unfortunately leads to zero sensitivity ($\chi = 0$). However, sensitivity can be increased by decreasing E_0 , which requires increasing ϵ in order to

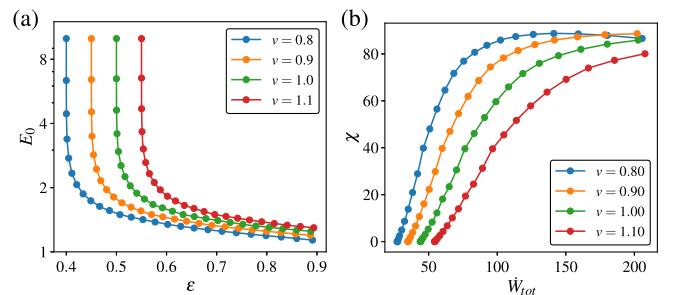


FIG. 3. The energy-speed-sensitivity trade-off in the two-site AIM. (a) Contours for constant v in the (ϵ, E_0) plane. (b) The total dissipation and sensitivity along different v contours. $N = 40$, $D = \omega = 1$.

maintain a fixed v [Fig. 3(a)]. As a result, \dot{W}_m and thereby the total dissipation increases. Figure 3(b) demonstrates this trade-off whereby enhancing sensitivity at a constant flocking speed necessarily increases dissipation. Similarly, for a given sensitivity, increasing the flocking speed also requires more dissipation; for a given dissipation, increasing speed necessarily reduces sensitivity (see the Supplemental Material, Sec. II [33] for analytical expressions). These relations constitute an energy-speed-sensitivity trade-off, which may affect the strategy for flocks (natural or artificial) to optimize their performance with limited resources.

Discussion and future directions.—A heuristic argument for the long-range order in the hydrodynamics theory of flocking (Toner-Tu equation) was the stabilizing effect of the convective term, which enables particles to change their neighborhoods of interaction [7]. Our study suggests that such a stabilizing mechanism that combines motion and alignment is intrinsically out of equilibrium and must be sustained by continuous energy dissipation (\dot{w}_a). Specifically, the motion leads to particle number fluctuations which, as shown by Eq. (6), directly causes energy dissipation. The fluctuation is maximal at the transition, resulting in the dissipation maximum. Therefore, the dissipation maximum reported here is deeply connected to the underlying mechanism that leads to flocking transition. Given that the same mechanism underlies general flocking models, it will be interesting to extend this study to flocking theories with continuous symmetry and off-lattice models [6–8]. In fact, a recent study on the Vicsek model also finds dissipation maximum near flocking transition, which suggests that the phenomenon observed in this study may be general [40]. Another possible direction is to compare the energy cost of flocking to other models of nonequilibrium phase transitions, some of which also demonstrate reduced energy dissipation in the ordered phase [41].

The two-site (and three-site) AIM provides a useful approach for understanding spatially extended nonequilibrium systems without completely going to the mean-field limit, which is an equilibrium limit unable to capture many nonequilibrium properties such as energy dissipation and the flocking transition. Given that the two-site AIM can be considered as a coarse-grained version of the full AIM, it will be interesting to investigate what is the appropriate coarse-graining procedure that preserves the dissipation characteristics, in particular, the cusped maximum behavior, and whether there is a scaling law for the dissipation, as suggested by recent studies of general reaction networks [28–30]. Finally, the energy-speed-sensitivity trade-off uncovered here may provide a useful perspective for understanding dynamics of natural flocks and designing optimal control of artificial flocks.

This work is supported in part by National Institutes of Health Grant No. R35GM131734 (to Y. T.). Q. Y. acknowledges the IBM Exploratory Science Councils for a summer internship during which the work was finished. Q. Y. acknowledges helpful discussions with D. Zhang, Q. Ouyang, C. Tang, L. Di Carlo, and C. Wu.

Appendix A: Energy dissipation in the 2D AIM.—The dynamics of the 2D AIM is simulated using the random-sequential-update algorithm outlined in the original model [12]. The steady-state energy dissipation rate is obtained by computing the average energy dissipation rate of a sufficiently long trajectory [34],

$$\dot{W} = \lim_{\tau \rightarrow +\infty} \frac{1}{\tau} \ln \frac{\mathcal{P}}{\mathcal{P}^R} = \lim_{\tau \rightarrow +\infty} \frac{1}{\tau} \sum_{i=0}^{M-1} \ln \frac{\tilde{k}_i}{\tilde{k}_i^R}, \quad (\text{A1})$$

where \mathcal{P} and \mathcal{P}^R are the probabilities of observing the forward and backward trajectories [42]. The trajectory contains M transitions (flipping or hopping), with \tilde{k}_i and \tilde{k}_i^R being the forward and backward transition rates of the i th transition (for a single spin). Thus, the rate ratios for flipping and hopping reactions can be summed separately, which leads to the partition between alignment and motion dissipation. For hopping, the log rate ratio $\ln(\tilde{k}_i/\tilde{k}_i^R)$ is simply $s\Delta x \ln[(1+\epsilon)/(1-\epsilon)]$, where $\Delta x = \pm 1$ is the displacement in the x direction. Hopping is along the bias when s and Δx have the same sign, which leads to positive dissipation. Conversely, hopping against the bias leads to negative dissipation. Hopping in the y direction does not contribute to dissipation since forward and backward rates are equal. Therefore, the motion dissipation rate is

$$\dot{W}_m = \lim_{\tau \rightarrow +\infty} \frac{1}{\tau} \sum_{0 < t < \tau} \Delta x s \ln \frac{1+\epsilon}{1-\epsilon} = N v_0 \ln \frac{1+\epsilon}{1-\epsilon}, \quad (\text{A2})$$

where $v_0 = 2D\epsilon$ is the average speed along the bias. Similarly, the forward and backward flipping rates are

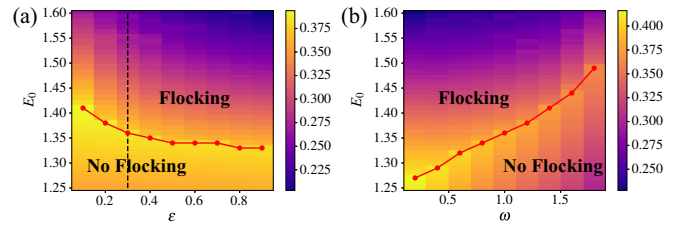


FIG. 4. Generality of the alignment dissipation maximum at flocking transition. The heat maps show the alignment dissipation density $\dot{w}_a/(L_x L_y)$ for different combinations of (a) (E_0, ϵ) and (b) (E_0, ω) . The red lines indicate the flocking transition as measured by the flocking velocity v . $D = 1$, $L_x = 300$, $L_y = 100$, $\bar{\rho} = N/(L_x L_y) = 5$. $\omega = 1$ for (a); $\epsilon = 0.3$ for (b). The black dashed line in (a) shows the parameter values for Fig. 1(b).

$\tilde{k}_i = \omega e^{-E_0 s m / \rho}$ and $\tilde{k}_i^R = \omega e^{E_0 s (m-2s) / \rho}$. The alignment dissipation is computed by summing the log ratios of the rates [Eq. (1)]. A more detailed discussion can be found in the Supplemental Material [33].

The generality of the alignment dissipation maximum at flocking transition shown in Fig. 1(b) is confirmed by simulation using different values of ϵ [Fig. 4(a)] and ω [Fig. 4(b)]. The red lines indicate the flocking transition E_c measured by the flocking velocity v , and the alignment dissipation density $\dot{w}_a / (L_x L_y)$ is quantified by the heat maps. In all cases studied, the dissipation maximum coincides with the flocking transition E_c , demonstrating generality of the result.

Appendix B: Analytical results in the two- and three-site AIM.—We start by computing \dot{w}_a for the two-site AIM. To obtain the steady-state distribution P^s , we decompose the linear operator \mathcal{L} into $\mathcal{L} = D\mathcal{L}_1 + \omega\mathcal{L}_2$, where \mathcal{L}_1 captures hopping transitions and \mathcal{L}_2 captures flipping [33]. The steady-state condition becomes $[\mathcal{L}_1 + (\omega/D)\mathcal{L}_2]P = 0$, where the second term is treated as a perturbation for small ω/D . To the leading order in ω/D , P can be written as

$$P = Q_0(a_0) \left(p_0 + \frac{\omega}{D} p_1 \right) + \mathcal{O}\left(\frac{\omega}{D}\right)^2, \quad (\text{B1})$$

where $p_0 = 2^{-N} \binom{a_0}{a_1} \binom{N-a_0}{b_1}$ is the solution to the hopping operator (i.e., $\mathcal{L}_1 p_0 = 0$), and $Q_0(a_0)$ captures the distribution of the total magnetization due to flipping. Q_0 and p_1 are determined by expanding $\mathcal{L}P = 0$ to $\mathcal{O}(\omega/D)$,

$$\mathcal{L}_2(Q_0 p_0) + \mathcal{L}_1(Q_0 p_1) = 0. \quad (\text{B2})$$

$$\sigma = \frac{1}{2\omega E_0} \sum_{\text{flip}} (J_+ - J_-) \ln \frac{k_+}{k_-} = 2E_0 z(1-z)^2 e^{E_0(2z-1)} \left(4z(1-z) - \frac{\omega \psi_1}{D} \right) N(x-y)^2 + \mathcal{O}(x^4, y^4), \quad (\text{B7})$$

where the higher-order terms in x and y are omitted since their expectation value vanishes in the infinite N limit. Importantly, σ vanishes exactly at the saddle point $(x, y, z) = (0, 0, z^*)$. Therefore, \dot{w}_a comes from the second-order term $N(x-y)^2$. This expansion directly relates \dot{w}_a to the particle number fluctuations since x and y are the continuum versions of a_1 and b_1 . The saddle point integral

$$\dot{w}_a = \begin{cases} E_0 \left(1 + \frac{\omega}{2D} (E_0 - 1) + \mathcal{O}\left(\frac{\omega}{D}\right)^2 \right), & E_0 < 1. \\ 8E_0 (z^*)^{3/2} (1-z^*)^{3/2} \left[1 + \frac{\omega}{2D} \left(2E_0 \sqrt{z^*(1-z^*)} - \frac{1}{2\sqrt{z^*(1-z^*)}} \right) + \mathcal{O}\left(\frac{\omega}{D}\right)^2 \right], & E_0 > 1. \end{cases} \quad (\text{B9})$$

First, we eliminate \mathcal{L}_1 by summing over a_1 and b_1 , which leads to the steady-state condition for Q_0 ,

$$\sum_{a_1, b_1} \mathcal{L}_2(p_0 Q_0) = 0, \quad \forall a_0. \quad (\text{B3})$$

In the infinite N limit, the solution is $Q_0(z) = e^{-F}$, where $z = a_0/N$ is the fraction of spin-up and F is the effective free energy given by Eq. (3). p_1 is determined by substituting the Q_0 solution into Eq. (B2),

$$p_1 = p_0 \frac{E_0}{4} \psi_1 [z(1-z)N(x-y)^2 - 1], \quad (\text{B4})$$

where $x = 2a_1/a_0 - 1$ and $y = 2b_1/(N - a_0) - 1$, and

$$\psi_1 = z e^{E_0(1-2z)} + (1-z) e^{-E_0(1-2z)}. \quad (\text{B5})$$

The total steady-state energy dissipation (entropy production) rate is

$$\dot{W}_{\text{tot}} = \sum_{i < j} (J_{i \rightarrow j} - J_{j \rightarrow i}) \ln \frac{k_{i \rightarrow j}}{k_{j \rightarrow i}}, \quad (\text{B6})$$

where the summation goes over all pairs of transitions (i, j) , which enables the decomposition into \dot{W}_m and \dot{W}_a by summing flipping and hopping transitions separately. For the motion dissipation, the calculation recovers Eq. (A2). The alignment dissipation is given by the expectation value of the dissipation rate density σ [defined in Eq. (5)],

in the (x, y) directions is done by averaging $N(x-y)^2$ over $[p_0 + (\omega/D)p_1]$,

$$\langle N(x-y)^2 \rangle = \frac{1}{z(1-z)} \left(1 + \frac{\omega E_0}{2D} \psi_1 \right). \quad (\text{B8})$$

The integral in the z direction is trivial since z can simply take its saddle point value. The result is

These expressions explicitly demonstrate how the alignment dissipation depend on both E_0 and the relative timescale ω/D . They are in good agreement with results obtained from the numerical solution of the master equation (see Fig. S6 in the Supplemental Material [33]). \dot{w}_a exhibits a cusped maximum at $E_c = 1$ regardless of ω/D because both the leading-order term and the correction term have discontinuous first derivatives there. The $\mathcal{O}(\omega/D)$ term is not included in the comparison with the 2D AIM [Fig. 2(b)] since the time needed to diffuse through the whole system is much longer than the timescale for flipping in the full model.

The three-site AIM can be solved by using the same method. The main difference is that the hopping

operator \mathcal{L}_1 explicitly depends on the bias ϵ , which enables us to capture the ϵ dependence of \dot{w}_a . Two new variables a_2 and b_2 are introduced for the number of + and - spins on site 2. To the first order in ω/D , the steady-state distribution is $P^s = Q_0(a_0)[p_0 + (\omega/D)p_1]$, where $p_0 = 3^{-N} \binom{a_0}{a_1} \binom{a_0-a_1}{a_2} \binom{b_0}{b_1} \binom{b_0-b_1}{b_2}$ is the solution to the hopping operator (i.e., $\mathcal{L}_1 p_0 = 0$). $Q_0 = e^{-F}$ is the same as that of the two-site model, and so is the saddle point z^* . The correction p_1 depends on both E_0 and ϵ , with its full expression given in the Supplemental Material [33]. The alignment dissipation is calculated using the saddle point method, which involves expanding to the second order in particle numbers. The result is

$$\dot{w}_a = \begin{cases} 2E_0 \left(1 + \frac{\omega}{D} \frac{6+\epsilon^2}{3(3+\epsilon^2)} (E_0 - 1) + \mathcal{O}\left(\frac{\omega}{D}\right)^2\right), & E_0 < 1, \\ 16E_0 (z^*)^{3/2} (1 - z^*)^{3/2} \left[1 + \frac{\omega}{D} \frac{6+\epsilon^2(2-4z^*(1-z^*))}{3(3+\epsilon^2)} \left(2E_0 \sqrt{z^*(1-z^*)} - \frac{1}{2\sqrt{z^*(1-z^*)}}\right) + \mathcal{O}\left(\frac{\omega}{D}\right)^2\right], & E_0 > 1. \end{cases} \quad (\text{B10})$$

In addition to capturing the cusped maximum at the transition, the three-site result also reveals how \dot{w}_a depends on ϵ . It is in good agreement with numerical results obtained using the Gillespie algorithm [43] (see Fig. S7 in the Supplemental Material [33]).

-
- [1] J. Toner, Y. Tu, and S. Ramaswamy, Hydrodynamics and phases of flocks, *Ann. Phys. (Amsterdam)* **318**, 170 (2005).
 - [2] S. Ramaswamy, The mechanics and statistics of active matter, *Annu. Rev. Condens. Matter Phys.* **1**, 323 (2010).
 - [3] M. C. Marchetti, J. F. Joanny, S. Ramaswamy, T. B. Liverpool, J. Prost, M. Rao, and R. A. Simha, Hydrodynamics of soft active matter, *Rev. Mod. Phys.* **85**, 1143 (2013).
 - [4] W. Bialek, A. Cavagna, I. Giardina, T. Mora, E. Silvestri, M. Viale, and A. M. Walczak, Statistical mechanics for natural flocks of birds, *Proc. Natl. Acad. Sci. U.S.A.* **109**, 4786 (2012).
 - [5] A. Kaiser, A. Snezhko, and I. S. Aranson, Flocking ferromagnetic colloids, *Sci. Adv.* **3**, e1601469 (2017).
 - [6] T. Vicsek, A. Czirok, E. Ben-Jacob, I. Cohen, and O. Shochet, Novel Type of Phase Transition in a System of Self-Driven Particles, *Phys. Rev. Lett.* **75**, 1226 (1995).
 - [7] J. Toner and Y. Tu, Long-Range Order in a Two-Dimensional Dynamical XY Model: How Birds Fly Together, *Phys. Rev. Lett.* **75**, 4326 (1995).
 - [8] J. Toner and Y. Tu, Flocks, herds, and schools: A quantitative theory of flocking, *Phys. Rev. E* **58**, 4828 (1998).
 - [9] G. Grégoire and H. Chaté, Onset of Collective and Cohesive Motion, *Phys. Rev. Lett.* **92**, 025702 (2004).
 - [10] H. Chaté, F. Ginelli, G. Grégoire, and F. Raynaud, Collective motion of self-propelled particles interacting without cohesion, *Phys. Rev. E* **77**, 046113 (2008).

-
- [11] A. P. Solon and J. Tailleur, Revisiting the Flocking Transition Using Active Spins, *Phys. Rev. Lett.* **111**, 078101 (2013).
 - [12] A. P. Solon and J. Tailleur, Flocking with discrete symmetry: The two-dimensional active Ising model, *Phys. Rev. E* **92**, 042119 (2015).
 - [13] F. S. Gnesotto, F. Mura, J. Gladrow, and C. P. Broedersz, Broken detailed balance and non-equilibrium dynamics in living systems: A review, *Rep. Prog. Phys.* **81**, 066601 (2018).
 - [14] G. Lan, P. Sartori, S. Neumann, V. Sourjik, and Y. Tu, The energy-speed-accuracy trade-off in sensory adaptation, *Nat. Phys.* **8**, 422 (2012).
 - [15] J. J. Hopfield, Kinetic proofreading: A new mechanism for reducing errors in biosynthetic processes requiring high specificity, *Proc. Natl. Acad. Sci. U.S.A.* **71**, 4135 (1974).
 - [16] J. Ninio, Kinetic amplification of enzyme discrimination, *Biochimie* **57**, 587 (1975).
 - [17] C. H. Bennett, Dissipation-error tradeoff in proofreading, *BioSystems* **11**, 85 (1979).
 - [18] A. Murugan, D. A. Huse, and S. Leibler, Speed, dissipation, and error in kinetic proofreading, *Proc. Natl. Acad. Sci. U.S.A.* **109**, 12034 (2012).
 - [19] P. Sartori and S. Pigolotti, Thermodynamics of Error Correction, *Phys. Rev. X* **5**, 041039 (2015).
 - [20] Q. Yu, A. B. Kolomeisky, and O. A. Igoshin, The energy cost and optimal design of networks for biological discrimination, *J. R. Soc. Interface* **19**, 20210883 (2022).
 - [21] G. Falasco, R. Rao, and M. Esposito, Information Thermodynamics of Turing Patterns, *Phys. Rev. Lett.* **121**, 108301 (2018).
 - [22] Y. Cao, H. Wang, Q. Ouyang, and Y. Tu, The free-energy cost of accurate biochemical oscillations, *Nat. Phys.* **11**, 772 (2015).
 - [23] H. Chaté, Dry Aligning Dilute Active Matter, *Annu. Rev. Condens. Matter Phys.* **11**, 189 (2020).

- [24] T. Markovich, É. Fodor, E. Tjhung, and M.E. Cates, Thermodynamics of Active Field Theories: Energetic Cost of Coupling to Reservoirs, *Phys. Rev. X* **11**, 021057 (2021).
- [25] U. Seifert, Stochastic thermodynamics, fluctuation theorems and molecular machines, *Rep. Prog. Phys.* **75**, 126001 (2012).
- [26] C. Nardini, É. Fodor, E. Tjhung, F. van Wijland, J. Tailleur, and M.E. Cates, Entropy Production in Field Theories without Time-Reversal Symmetry: Quantifying the Non-Equilibrium Character of Active Matter, *Phys. Rev. X* **7**, 021007 (2017).
- [27] É. Fodor, R.L. Jack, and M.E. Cates, Irreversibility and biased ensembles in active matter: Insights from stochastic thermodynamics, *Annu. Rev. Condens. Matter Phys.* **13**, 215 (2022).
- [28] Q. Yu, D. Zhang, and Y. Tu, Inverse Power Law Scaling of Energy Dissipation Rate in Nonequilibrium Reaction Networks, *Phys. Rev. Lett.* **126**, 080601 (2021).
- [29] Q. Yu and Y. Tu, State-space renormalization group theory of nonequilibrium reaction networks: Exact solutions for hypercubic lattices in arbitrary dimensions, *Phys. Rev. E* **105**, 044140 (2022).
- [30] L. Cocconi, G. Salbreux, and G. Pruessner, Scaling of entropy production under coarse graining in active disordered media, *Phys. Rev. E* **105**, L042601 (2022).
- [31] É. Fodor, C. Nardini, M.E. Cates, J. Tailleur, P. Visco, and F. van Wijland, How Far from Equilibrium Is Active Matter?, *Phys. Rev. Lett.* **117**, 038103 (2016).
- [32] ø.L. Borthne, É. Fodor, and M.E. Cates, Time-reversal symmetry violations and entropy production in field theories of polar active matter, *New J. Phys.* **22**, 123012 (2020).
- [33] See Supplemental Material at <http://link.aps.org/supplemental/10.1103/PhysRevLett.129.278001> for details on the calculation of energy dissipation in the 2D AIM and solutions of the two- and three-site AIM.
- [34] L. Peliti and S. Pigolotti, *Stochastic Thermodynamics: An Introduction* (Princeton University Press, Princeton, NJ, 2021).
- [35] T.L. Hill, *Free Energy Transduction in Biology: The Steady-State Kinetic and Thermodynamic Formalism* (Academic Press, New York, 1977).
- [36] H. Qian, Open-system nonequilibrium steady state: Statistical thermodynamics, fluctuations, and chemical oscillations, *J. Phys. Chem. B* **110**, 15063 (2006).
- [37] From the perspective of coarse graining, the flocking phase of the two-site model includes both the mixed phase and the liquid phase of the full AIM.
- [38] Y. Kuramoto, *Chemical Oscillations, Waves, and Turbulence* (Springer Berlin, Heidelberg, 2003), 10.1007/978-3-642-69689-3.
- [39] D. Zhang, Y. Cao, Q. Ouyang, and Y. Tu, The energy cost and optimal design for synchronization of coupled molecular oscillators, *Nat. Phys.* **16**, 95 (2020).
- [40] F. Ferretti, S. Grosse-Holz, C. Holmes, J.L. Shivers, I. Giardina, T. Mora, and A. Walczak, Signatures of irreversibility in microscopic models of flocking, *Phys. Rev. E* **106**, 034608 (2022).
- [41] T. Herpich, J. Thingna, and M. Esposito, Collective Power: Minimal Model for Thermodynamics of Nonequilibrium Phase Transitions, *Phys. Rev. X* **8**, 031056 (2018).
- [42] The spin variables do not change sign under time reversal.
- [43] D.T. Gillespie, Exact stochastic simulation of coupled chemical reactions, *J. Phys. Chem.* **81**, 2340 (1977).